Heliyon

Received:
15 February 2017
Revised:
4 June 2017
Accepted:
12 July 2017

Cite as: Jens Seedorf, Ralf-Gunther Schmidt. The simulated air flow pattern around a moving animal transport vehicle as the basis for a prospective biosecurity risk assessment. Heliyon 3 (2017) e00358. doi: 10.1016/j.heliyon.2017.e00358

The simulated air flow pattern around a moving animal transport vehicle as the basis for a prospective biosecurity risk assessment

Jens Seedorf [a,*], **Ralf-Gunther Schmidt** [b]

[a] *Unit of Animal Hygiene and Food Safety, University of Applied Sciences Osnabrück, Osnabrück, Germany*

[b] *Laboratory for Fluid Mechanics and Turbomachinery, University of Applied Sciences Osnabrück, Osnabrück, Germany*

* Corresponding author.

E-mail address: j.seedorf@hs-osnabrueck.de (J. Seedorf).

Abstract

Research that investigates bioaerosol emissions from animal transport vehicles (ATVs) and their importance in the spread of harmful airborne agents while the ATVs travel on roads is limited. To investigate the dynamical behaviour of theoretically released particles from a moving ATV, the open-source computational fluid dynamics (CFD) software OpenFOAM was used to calculate the external and internal air flow fields with passive and forced ventilated openings of a common ATV moving at a speed of 80 km/h. In addition to a computed flow rate of approximately 40,000 m^3/h crossing the interior of the ATV, the visualization of the trajectories has demonstrated distinct patterns of the spatial distribution of potentially released bioaerosols in the vicinity of the ATV. Although the front openings show the highest air flow to the outside, the recirculations of air masses between the interior of the ATV and the atmosphere also occur, which complicate the emission and the dispersion characterizations. To specify the future emission rates of ATVs, a database of bioaerosol concentrations within the ATV is necessary in conjunction with high-performance computing resources to simulate the potential dispersion of bioaerosols in the environment.

http://dx.doi.org/10.1016/j.heliyon.2017.e00358

Keywords: Environmental science, Veterinary science, Civil engineering, Public health

1. Introduction

Biosecurity in livestock production is defined as the implementation of measures that reduce the risk of introduction and spread of disease agents. The airborne transmission of bioaerosols is a possible method by which infections move from farm to farm [1]. Therefore, the physical location of herds should be carefully planned to maintain adequate distances from neighbouring farms and frequently used roads, as vehicles can also be instrumental in spreading animal diseases [2]. Consequently, longer transport distances of animals are associated with a higher likelihood of the geographical spread of animal diseases or even zoonotic agents. Unfortunately, the role of animal transport vehicles (ATVs) as considerable emitters of airborne and infective microorganisms is not well-documented [3, 4], or is associated to public health issues only [5]. For instance, the outbreak of classical swine fever in The Netherlands in 1997 was spread by transport vehicles on some occasions [6]. Conversely, an unambiguous connection could not be demonstrated between disease outbreak and pathogen dissemination by a transport lorry [7]. Despite the uncertainties and knowledge gaps in this area, emerging pathogens (such as African swine fever [8] or porcine epidemic diarrhoea [9]), as part of bioaerosols, generally possess the ability to spread via airborne routes. The awareness of this emission and transmission events was actually reflected by precautionary investigations in poultry barns, which were located at a maximum distance of 500 m at the right and left sides of roads due to the long-distance transport of a suspected avian influenza-positive poultry herd in a ground vehicle to a slaughterhouse in 2014 [10]. This evidence indicates that the transportation of pathogen shedding farm animals can potentially cause devastating epidemics in a spatial context.

Established numerical dispersion models predict the atmospheric distribution of infective particle plumes [11]. Computational fluid dynamics (CFD) is a suitable prediction tool for bioaerosol emitting and moving vehicles. CFD delivers data even if measurements are difficult or expensive or experiments are not possible [12]. This method was recently used to calculate the air flow pattern for a geometrical simplified truck [13].

The long-term aim of the study is to show the general dispersion pattern of bioaerosols, which are potentially released from a moving ATV. At this stage of our investigations we calculate by means of a CFD simulation the air flow field both inside and outside of a common trailer for pig transportation with passive and forced ventilated openings. The escaping air fluxes at each opening of the trailer were also investigated as an additional prerequisite for prospective bioaerosol

http://dx.doi.org/10.1016/j.heliyon.2017.e00358

emissions and transmissions. This procedure is employed to assess the exposure and subsequent infection risk for livestock herds in the vicinity of roads and motorways in the future, as fundamentally shown in an animated virtual scene in Supplementary Movie 1.

2. Methods

Truck and corresponding gooseneck-trailer models were created using computer-aided design software (Fig. 1). The proportions and characteristic features were obtained from 2D construction plans of a commercially available three-level trailer for pig transportation. Thus, the position and size of the loading compartments, partition walls and ventilation openings were closely modelled to the same parts of a real trailer. Additionally, the reduced air volume within the trailer due to the transported animals must be represented as it influences the air flow pattern [14]. From this point of view, pigs were only considered to have box-like geometric shapes, which occupied each loading level. The occupied volume of this replacement geometry was identical to the expected fully loaded livestock volume. Therefore, the inner volume of the truck was accurately matched to the inner volume in real usage conditions. The simplification of the bodies of pigs was a compromise to the exact flow modelling of the inner compartment, which could only be approximated, as the position and stance of each individual pig could only be assumed. The exact modelling of the bodies of pigs may also considerably increase the computation time due to the expected higher cell numbers of the

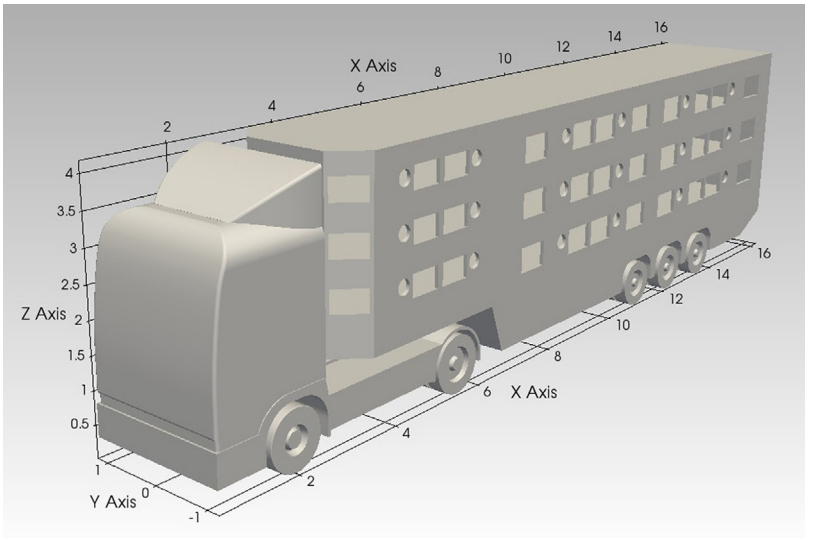

Fig. 1. Architecture and dimension of the ATV in metres. Left side view of the ATV model was composed of a truck in the front and a gooseneck-trailer for pig transportation in the back. The round openings were installed with fans (diameter: 246.4 mm), whereas the rectangular openings (621 × 450 mm and 662 × 450 mm, respectively) were installed without fans.

http://dx.doi.org/10.1016/j.heliyon.2017.e00358

domain. The surface of the geometry that replaced the bodies of the pigs was positioned at the pigs' waist level and served as a potential emission source for the bioaerosol particles. On this surface, the emission concentration (relative volumetric densities of the bioaerosols) was theoretically defined as 100%.

To follow the virtual particles on the trajectories surrounding the ATV, the airborne emission was traced by a solution of a convection-related passive scalar transport equation based on the velocity field. The diffusion processes were neglected as the velocity was the predominant emission determining influence. Particle size distributions and particle size-related densities for released bioaerosols from ATVs were not considered due to the absence of valid data to our knowledge. But particle specific data would be necessary to take into account the sedimentation of particles, for example, and to be subsequently able to derive the net emission. As a compromise and to visualize a plume at least, particles were modelled as massless and did not affect the air flow pattern.

The resulting emission field can be interpreted as a relative particle concentration compared with the particle concentration directly on the pig's surface. The spatial distribution of the particles (i.e., bioaerosol) within the domain determines the percentage of potential bioaerosols exiting the virtual wind tunnel and spreading into the environment.

The appropriate internal ventilation was maintained by 18 fans, which caused a general air flow from outside to inside, and 33 lockable hatches with shutters, which were considered to be fully open to allow maximum air exchange. Each hatch prevented the escape of animals by three metal bars, which were neglected in the simulation model as the cross-section of the metal bars in relation to the free cross-section of a hatch was small (cross-sectional obstruction level $< 5\%$).

The animals were protected from the fans by perforated plates with a cross-sectional obstruction level of nearly 50%, which caused an additional pressure loss, and therefore, significantly changed the fan characteristics in relation to the characteristics provided by the fan manufacturer. The fans, which are operated with a constant fan power level of 100%, were modelled in the simulation as a pressure jump boundary condition with a polynomial function depending on the velocity normal to the fan openings. The pressure loss induced by the perforated plates was considered by reducing the provided fan performance characteristics. This pressure loss was calculated from the geometry by empirical formulas for perforated plates [15].

The calculations of the velocity, pressure, turbulence and emission fields were conducted using the open-source CFD program OpenFOAM 2.3.0. Among the diverse available CFD solvers, the κ-ω model is appropriate for automotive simulations due to its balance of computational efficiency and accuracy. The κ-ω

http://dx.doi.org/10.1016/j.heliyon.2017.e00358

model is sufficiently accurate for more turbulent applications with greater pressure gradients that are similar to the conditions, which frequently occur at moving vehicles [16]. Additionally, the applicability of the OpenFOAM for flow simulations was outlined by Chen et al. [12]. From this point of view and to suitably consider turbulences, the Reynolds Averaged Navier-Stokes equations (RANS) were solved in conjunction with Menter's Shear Stress Transport (κ-ω-SST) turbulence model. As the maximum Mach number within the domain was 0.12, the compressibility effects were neglected. The turbulence intensity at the inlet of the virtual wind tunnel has been set to 1.8% [17]. A comprehensive manual and the physical basics for the CFD program OpenFOAM are available online (http://www.openfoam.org).

The flow simulations were performed for varying sizes of the virtual wind tunnel to prevent falsification of the results due to wall-object interactions. The size of the wind tunnel was increased until the change in the drag coefficient of the entire model was less than 0.7%. This problem was mirrored around the X-Z-plane at the Y-position = 0 using a symmetric boundary condition. The virtual wind tunnel dimensions were set to 240 × 80 × 40 metres, which approximately corresponded to five model lengths between the inlet and the object, ten model lengths between the object and outlet and five model lengths between the symmetry plane and the side wall.

To avoid the overdetermination of the equations, the classical approach of a fixed velocity at the inlet and a fixed pressure at the outlet, each in conjunction with a zero gradient boundary for the other field variable, was employed. The movement of the vehicle was simulated at 22.22 m/s (80 km/h), which was chosen as the inlet air velocity for the wind tunnel. The lower wall of the wind tunnel was modelled as a moving wall; its velocity corresponds to the velocity of the approaching flow. The top and side walls were fitted with a slip condition, which prevented normal flow and prevented the simultaneous generation of friction.

For mesh creation, the tool snappyHexMesh was used. This tool created unstructured hexahedron meshes (Fig. 2). All truck and trailer surfaces were resolved with an accuracy of a 15-mm element edge length and were equipped with ten surface layers, each with a thickness of 2 mm. A sphere with a distance from the model's surface of 2 m was resolved with a resolution of 31 mm. In addition, all cells with a distance from the surface of 4 m were resolved with a minimum resolution of 62 mm.

A complete grid independence analysis was performed. The parameters of grid generation (the resolution of the geometry, the number of wall layers and the size of the refinement area) were varied until the change in the drag coefficient was less than 2%. The final grid of the entire model consisted of 13 million cells.

http://dx.doi.org/10.1016/j.heliyon.2017.e00358

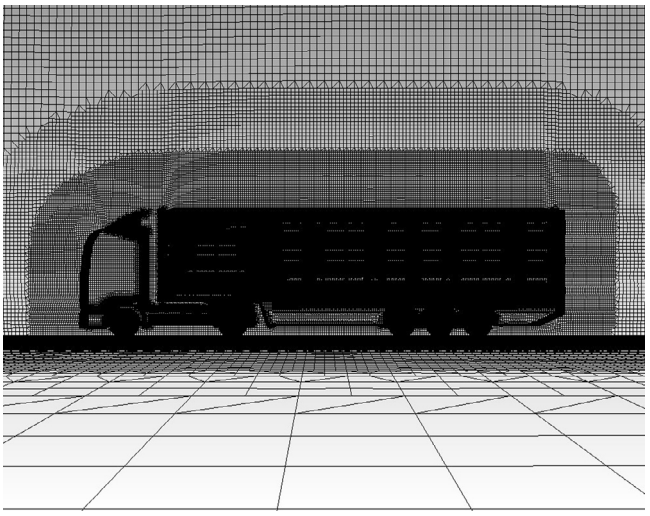

Fig. 2. General domain resolution for the simulation. An excerpt of the domain's mesh shows high grid resolution and spherical refinements that are similar to the ATV model.

After the initialization of the calculation with a completely parallel flow in all cells, the starting solutions for velocity and pressure fields were obtained with an inviscid potential solver. A decrease in the residuals of a minimum of seven orders was achieved. The results of this step were subsequently used as initial values for the solution of the RANS equations with a SIMPLE algorithm. This step considered both viscosity and turbulence. After 2,000 iterations, the flow field variables showed a decrease in the residuals of a minimum of three orders, where the solution converged. A total of 10,000 iterations were performed, and no significant effects on the field variables were observed.

The flow rates through the hatches and fans were obtained during post-processing by surface sampling, in which each opening was introduced as a meshed flat surface with equally oriented cell normal vectors into the numerical domain. The vector field of the flow velocity was evaluated by forming the scalar product of the normal vector of a cell with the flow velocity vector and an integration over the respective area of the openings. The streamlines were generated by the Runge–Kutta integration method, which was provided by the visualization software Paraview (http://www.paraview.org). This computer program was also used to illustrate the post-processed results.

3. Results and discussion

The pressure field around an ATV, which was generated by ambient wind and vehicle-induced air flow, is intentionally used to cause air movement through the ATV, to obtain an even distribution of fresh air, to remove moisture and heat and to guarantee appropriate thermoregulatory responses by the transported animals due

http://dx.doi.org/10.1016/j.heliyon.2017.e00358

to their physiological capabilities. Therefore, the application of CFD is a promising tool to better understand the ventilation characteristics of ATVs [14, 18] and to derive recommendations regarding the adaptation of a microclimate to the welfare demands of transported animals.

In addition to these pronounced welfare aspects, the air quality inside the vehicle, such as gases, dust and microorganisms, is also an important issue from an epidemiological point of view [19], as an ATV potentially interacts with its external environment due to its semi-open construction properties. Any trailer-related openings, with or without installed fans, serve not only as inlets for the ambient air with potentially infective agents [20] but also as outlets for airborne agents that originate from the transported animals and their liquid and solid discharges [21]. To support this hypothesis from a theoretical point of view, a numerical simulation of the air flow field can be used to visually and numerically demonstrate the dynamic interactions among a moving ATV, its potentially released bioaerosols and the surrounding air. Additionally, the spatial interaction of all inlets and outlets can be demonstrated as an important prerequisite to model the complex dispersion of particulate matter in the ambient air in the future and to understand the distribution of released bioaerosols into the environment. This finding is also useful to confirm or design appropriate field studies. Seo et al. [21] confirmed a transmission distance of particulate matter of nearly 80 m on the downwind side of the ATVs in a field study, in which the ATVs passed a set-up of measurement devices beside a road. However, the data availability of vehicle-associated bioaerosol concentration and emissions is currently very low, particularly with respect to the different livestock types that are generally transported on roads.

3.1. Visualization of the air flow pattern

The simulation corresponds with road vehicle aerodynamics studies [22]. The total air flow field, in this case, is comparable to ATVs with only passive ventilation, in which an external pressure field around the moving ATV provides the driving force for air exchange between the inner space of the transporter and the ambient space of the transporter. According to Kettlewell et al. [23], the air that passes over the front edges of the trailer separated from the vehicle and created a region of suction. The air flow re-attached along the length of the vehicle and at the rear openings. Although a region of suction remained, the magnitude of the suction was significantly less than the magnitude of the suction at the front openings. The net effect of this pressure field was that air tended to enter at the rear openings, moved forward within the trailer over the animals and exited through the front openings [24] (Fig. 3a). In contrast to this observation, the results in this paper indicated an outflow from the vehicle both at the neck and the end of the trailer. Simulations with active fans did not show substantial changes in the air flow pattern, but the

http://dx.doi.org/10.1016/j.heliyon.2017.e00358

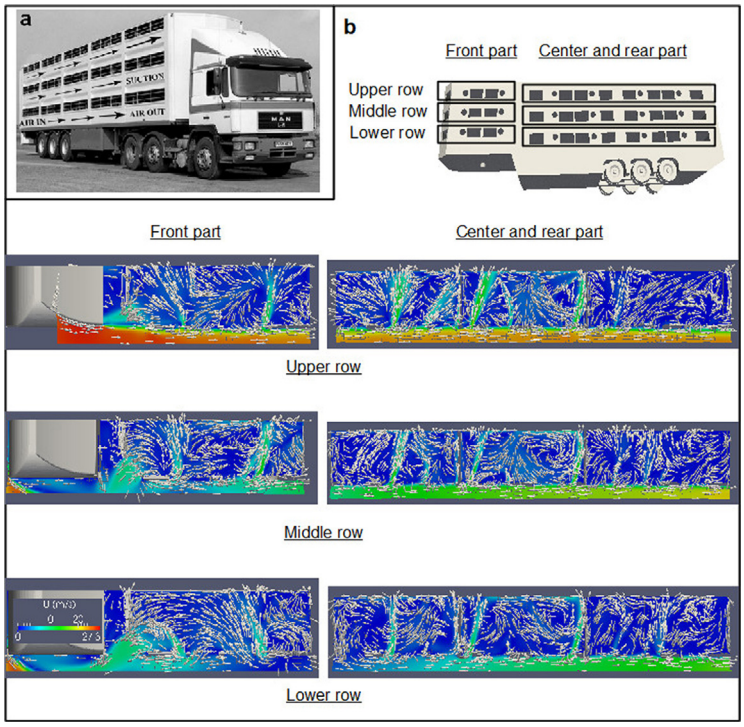

Fig. 3. General air flow behaviour in ATVs. (a) Air movement situation of a naturally ventilated straight livestock trailer with a solid headboard and standard side grille vents [24]. (b) Segmentation of the internal air flow field within the investigated ATV. Two-dimensional surface vectors (z = 0) indicates the calculated flow direction on three horizontal slices above the simplified bodies of pigs. The slices cross the openings along the lower, middle and upper rows of vents. Top view of the truck for spatial orientation.

total air exchange was considerably higher when the fans were enabled. The flow pattern within the inner sections is rather complex due to the interaction among the fans, the pig replacement geometries, the section divider walls (which allow airflow through some orifices and a slot at floor level) and the ambient pressure field (Fig. 3b). Texture-based flow visualization methods provide a unique means to address the limitations of depictions based on a limited set of streamlines or vectors as seen in Fig. 3b. These methods yield an effective, dense representation which conveys essential patterns of a vector field. The application of a line integral convolution filter is an appropriate measure to produce a dense set of streamline-type patterns that fill the domain [25]. Such a higher spatially resolved air flow pattern around and in the ATV shows Fig. 4a and b. It is clearly recognizable where vortices, diverging or converging air flows exist at the interfaces (e.g., vents) between the interior and exterior of the ATV. Particularly, the vortices within the ATV lead to the assumption that bioaerosols may then underlie impactional and interceptional forces, which partly influence the net emission (see also Ch. 3.3). In addition to Fig. 3 and 4 an overview of the ambient flow field and its vortex regions is shown in Fig. 5. These regions are obviously located in the

http://dx.doi.org/10.1016/j.heliyon.2017.e00358

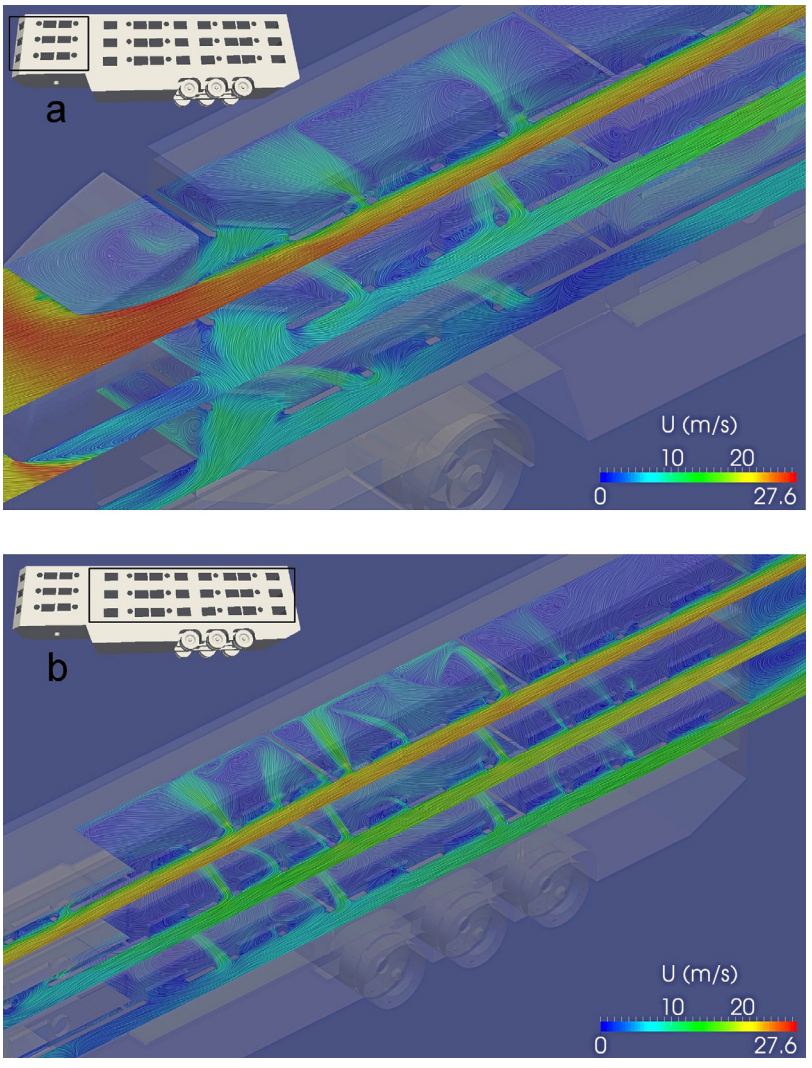

Fig. 4. Air stream conditions for the ATV at 80 km/h. (a) Air flow pattern in the front and (b) in the rear part of the animal transport vehicle (ATV) demonstrated by the surface associated line integral convolution plug-in of Paraview, which optimizes the spatial resolution of the air stream along and within ATV (use higher zoom factor for the document to see details more clearly). The black frame of the trailer pictograms indicates the location of the displayed air flow pattern.

vicinity of the front openings and at the rear part of the trailer. According to Fig. 6 the static pressure conditions along the ATV can be distinguished into zones with positive and negative pressures as air flow-driving forces.

3.2. Air flow through vent openings

The determination of air velocities provides an initial impression of the movement of air masses within the vent openings of the ATV (Fig. 7). These openings, which serve as air entering and air exiting openings in the chosen simulation conditions, should be identified. Although the front and the rear openings of the ATV clearly

http://dx.doi.org/10.1016/j.heliyon.2017.e00358

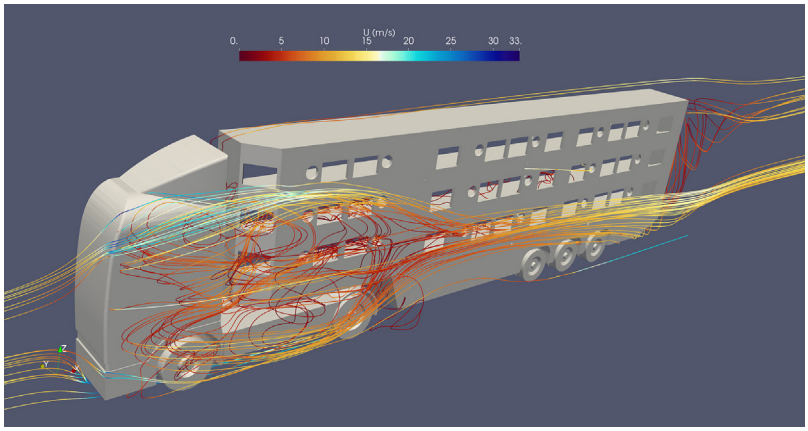

Fig. 5. Basic CFD results for the ATV. Calculated streamlines reveal expected vortex pattern at the truck-trailer gap and the truck's rear.

show air movement from inside to outside, the direction of the streaming air through the remaining openings is not distinct due to the heterogeneous air velocity profiles. Only the subsequent quantification of the volume flow rates clarifies the status of each opening to be addressed as inlets or outlets for air masses.

The calculated total air inflow rate (positive value) and outflow rate (negative value) through the vent openings of the ATV were 40412 m^3/h and −40790 m^3/h, respectively. The relative error of the flow rate calculation was 0.93%. For example, this error can be traced to the quality of the tessellation procedure that was applied for each of the vent openings. Consequently, small differences in the grid architecture may locally occur and influence the zonal boundary interfaces. These discontinuities on a grid can cause interpolation errors at the zonal

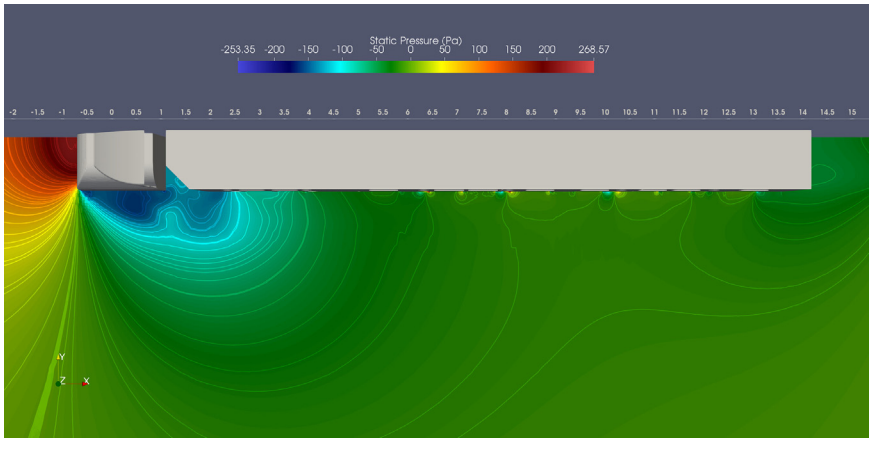

Fig. 6. Basic CFD results for the ATV. An excerpt of static pressure conditions for a horizontally sliced area along the ATV (top view). The visible contour lines indicate the spatial transition among the colourized pressure zones. The thin grey grid line represents the x-axis in metres.

http://dx.doi.org/10.1016/j.heliyon.2017.e00358

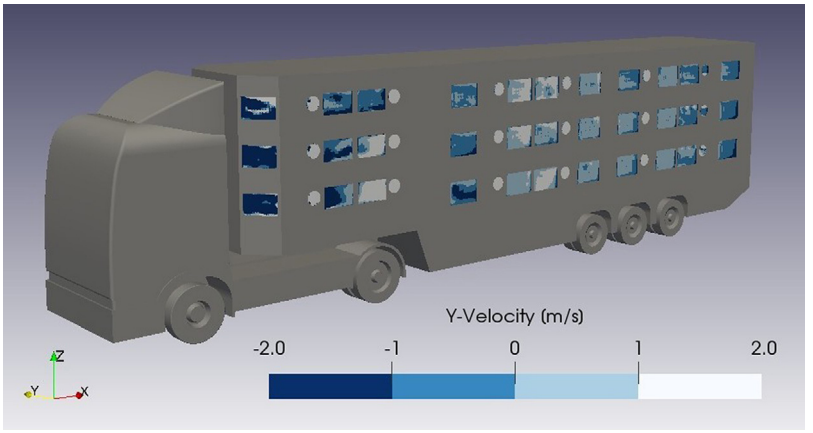

Fig. 7. Distribution of normal velocities within the hatches and fan openings of the ATV. Air velocities for inflow (positive values) and outflow (negative values) are illustrated for a speed of 80 km/h and 100% fan power.

interfaces, where the computed solution of one zone is approximated on the boundary of another zone [26].

As previously suggested in conjunction with Fig. 7, Fig. 8 shows that the highest air flow rates from inside to outside exist in the hatches U1, M1 and L1 directly behind the truck cabin, which is caused by the flow separation at the leading edges of the trailer. Behind the first column of hatches, the unforced outflow rates decreased and generally converted to unforced inflow through the hatches of the central compartment (UML8 and UML9). Concerning the rear compartment, the airflow between the interior of the ATV and the exterior of the ATV was nearly evenly distributed along the hatches. Although all fans in the front and central compartments showed comparable inflow values, the flow rates of the fans in the rear compartment (UML16) decreased to relatively low values. The flow rate of the fan in the upper deck (U16) evenly converted to a negative flow rate of 64.5 m^3/h, which indicates a flow direction from the inside of the trailer to the outside of the trailer, although all other active fans sucked air from the outside to ventilate the interior of the trailer. The hatches near the rear edges of the trailer (UML17) showed a flow direction from inside to outside. This was caused by the flow separation at the rear edges of the trailer with its large suction and vortex zone behind the rear wall (see Fig. 5). Due to its width and intensity, this zone embraces the rear edges of the trailer and induces a negative pressure in the upstream area.

3.3. Recirculation and relative emission of particles

The calculated quantitative and qualitative flow pattern showed that potentially existing bioaerosols were not exclusively emitted into the ambient air along the visualized trajectories. However, these airborne components were also able to re-

http://dx.doi.org/10.1016/j.heliyon.2017.e00358

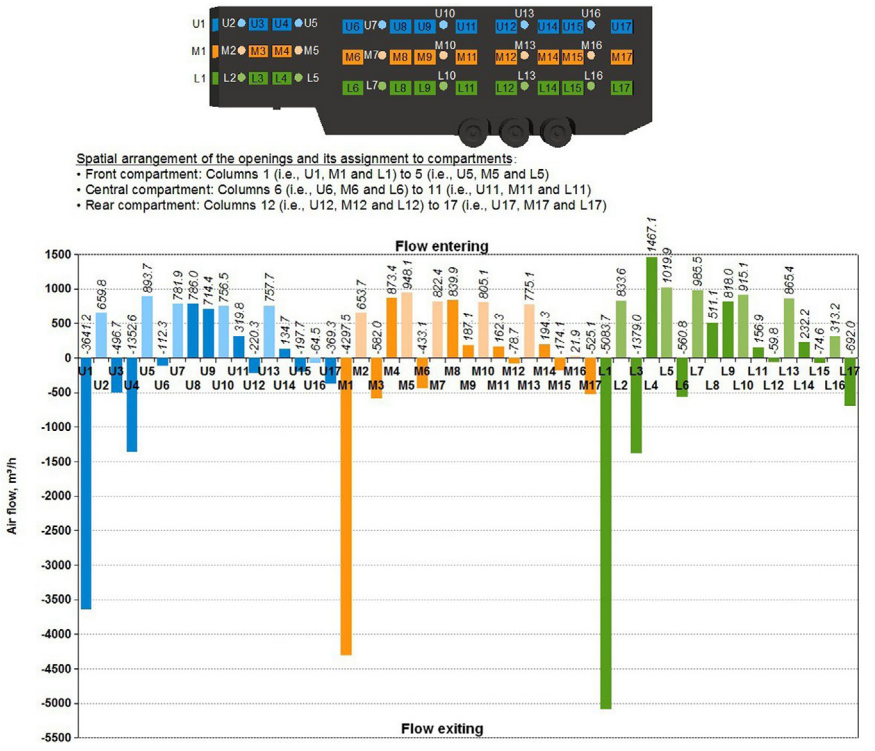

Fig. 8. Air flow rates (m^3/h) for hatches and fans at a vehicle speed of 80 km/h. Values are shown for one side of the ATV. Blue, orange and green vents of the trailer (refer to image) correspond with the bars of the same colour in the diagram. Fan-related (round openings) and passive ventilations (rectangular openings) are indicated by different contrasts of the same colour (brighter: fans, darker: hatches) in the bar graph and in the upper (U) rows, middle (M) rows and lower (L) rows, respectively, of the vents.

enter the trailer as the openings were spatially close with varying flow directions. Therefore, it can be assumed that bioaerosols recirculate between the interior of the ATV and the ambient air. The idea of a re-entry and recirculation phenomenon, is illustrated in Supplementary Movie 2, where animated virtual spheres (particles) follow spatially aligned streamlines of the CFD simulation. From this point of view, the net emission quantities from ATVs are difficult to determine as a simple multiplication of flow rates and any concentrations of bioaerosols in ATVs (if known), because this procedure does not reflect the realistic emission strength. The recirculation phenomenon and the dispersion behaviours of ATV-related bioaerosols were likely not adequately considered by user-friendly numerical atmospheric dispersion models (e.g., official Lagrangian particle dispersion models to assess the environmental impact of stationary emission sources, such as livestock buildings) or exactly recorded by measurements at or in the trailer, as the measurements were not able to distinguish between directly emitted bioaerosols and (temporarily) recirculating bioaerosols.

To overcome this bottleneck, CFD can be used to determine the net emission of bioaerosols despite recirculations. Bioaerosols, which will escape into the

http://dx.doi.org/10.1016/j.heliyon.2017.e00358

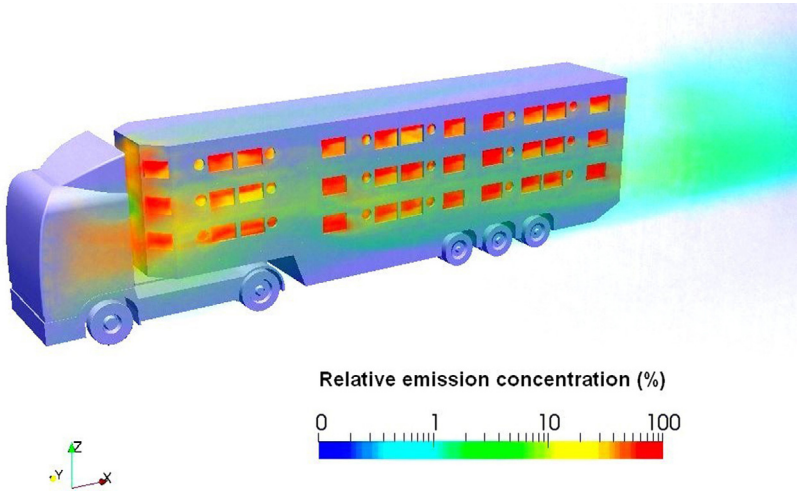

Fig. 9. Emission plume of the moving ATV. Volumetric display of the relative airborne emission concentration (0–100%) caused by the ATV. The emission concentration was set to 100% on the pig bodies' surfaces in the inner compartments of the trailer. The emitted bioaerosols show an uneven distribution near the ATV. According to the air exchange (Fig. 8) and the wall pressure distribution (Fig. 6), the highest emission concentration outside the ATV can be observed in the truck-trailer gap, from where the emissions are considerably transported behind the trailer by the ambient flow (Fig. 5). The original image was adjusted by colour contrast and saturation to sharpen the emission plume against the background.

environment, must leave the virtual wind tunnel through the outflow boundary. The recognizable emission plume in Fig. 9 indicates the previously mentioned circumstance in conjunction with dilution effects in the ambient air and shows that the relative emission concentration behind the trailer only consists of a fraction of the original relative emission concentrations of 100%. Only these completely released bioaerosols were transferable and potentially able to affect receptors in the neighbourhoods of the roads.

4. Conclusions

Understanding the dispersion behaviour of harmful components from livestock operations is a prerequisite for environment-related risk assessments [27]. In this context, the emission of bioaerosols from livestock buildings has become more important in recent years due to human- and animal-related epidemiological questions [28, 29]. The risk assessments in conjunction with moving ATVs are even more complicated in relation to not only adequate measurements in the field but also prediction tools, which calculate the dispersion and transmission of specific emitted components, such as pathogens. In contrast to typical dispersion models for stationary sources [30, 31], the application of CFD is necessary for solving the higher demands of the predictability of flow fields caused by mobile complex geometries.

http://dx.doi.org/10.1016/j.heliyon.2017.e00358

Although the CFD results should be validated against experiments [12, 32], the application of OpenFOAM in academic research and industry is commonly accepted [33]. OpenFOAM is deemed to be a reliable research solver in the field of bluff body flows, whereas, among RANS models, κ-ω-SST provides accurate results [34]. It is not necessary to maintain a specific format of reporting the CFD modelling, but best guidelines for CFD applications are desirable to ensure the quality of simulation results. However, sometimes it could be difficult to perform quality assurance studies to the full extent [32]. From this perspective, this paper attempts to preliminarily describe the behaviour of air flow in the vicinity of a moving ATV. The paper also investigates the likely influence of trajectories with laminar- and turbulence-related characteristics on potentially emitted particles, which determine the destinies of particles in the environment in relation to time and space. The calculated air flow pattern indicates the following main results with respect to the chosen simulation conditions:

- the passive ventilated front openings of the gooseneck-trailer show the highest volumetric outflow of air followed by the passive ventilated rear openings;
- the rear part of the trailer is expected to show a vortex region, which is capable of not only extracting air via the rear vent openings but also causing a flow inversion in one fan-equipped opening;
- the released particle-loaded air from the interior of the trailer is not exclusively diluted and forwarded by the ambient air but can partly re-enter the trailer via the vent apertures, which causes a recirculation of particles likely;
- due to the lack of particle-related emission concentrations, the calculation of relative emission concentrations indirectly indicates the proportion of released particles that definitely reach the environment.

The results let suggest, that prospective studies should consider additional ‘real world' aspects, such as peripheral buildings, vegetation, and oncoming traffic, because these structures and activities also significantly influence the dispersion of ATV-emitted airborne components that may reach receptors (i.e., farms) beside roads. In contrast to the symmetric flow conditions in this study, varying wind conditions, such as side wind, are additional relevant factors, which may significantly increase the release of bioaerosols. To consider these conditions, high-performance computing systems are necessary to fulfil the high demands on CPU performance and subsequently create a more realistic aerodynamic situation for ATVs on roads. This finding offers the possibility of optimizing CFD calculations, which renders the results more trustworthy due to refinements (e.g., modifications of the resolution and topologic characteristics of the meshes).

Apart from the necessity of initiating measurement campaigns to construct a database of ATV-related emission factors for particles, bioaerosols or pathogens,

http://dx.doi.org/10.1016/j.heliyon.2017.e00358

the results from prospective field studies can also help to verify the simulations if particle differentiating methods are developed to differentiate between ATV-related particles and naturally occurring particles in ambient air. Given these methods, calculated backward air trajectories can be employed to follow bioaerosols to their source and determine net emission quantities for an extensive range of different types of ATVs on roads. In the future, this inverse dispersion modelling approach can aid in building an emission inventory of bioaerosol-releasing vehicles.

Declarations

Author contribution statement

Jens Seedorf: Conceived and designed the analysis; Analyzed and interpreted the data; Contributed analysis tools or data; Wrote the paper.

Ralf-Gunther Schmidt: Contributed analysis tools or data; Interpreted the data; Wrote the paper.

Funding statement

This research did not receive any specific grant from funding agencies in the public, commercial, or not-for-profit sectors.

Competing interest statement

The authors declare no conflict of interest.

Additional information

Supplementary content related to this article has been published online at http://dx.doi.org/10.1016/j.heliyon.2017.e00358.

Acknowledgements

We thank our research assistant and the German companies Finkl and Venneker for their technical support.

References

[1] S. Dee, S. Otake, S. Oliveira, J. Deene, Evidence of long distance airborne transport of porcine reproductive and respiratory syndrome virus and *Mycoplasma hyopneumoniae*, Vet. Res. 40 (2009) 39–52.

[2] FAO, Food and Agriculture Organization of the United Nations/World Organisation for Animal Health/World Bank. Good practices for biosecurity

in the pig sector – Issues and options in developing and transition countries, FAO Animal Production and Health Paper No. 169, Rome, 2010, pp. 89.

[3] M. Greger, The long haul: Risks associated with livestock transport, Biosecur. Bioterror. 5 (2007) 301–311.

[4] J. Hartung, The new E.U. Animal Transport Regulation: Improved welfare and health or increased administration? Dtsch. Tierärztl. Wschr. 113 (2006) 113–116.

[5] A.M. Rule, S.L. Evans, E.K. Silbergeld, Food animal transport: A potential source of community exposures to health hazards from industrial farming (CAFOs), J. Infect. Public Health 1 (2008) 33–39.

[6] European Commission (EC), The welfare of animals during transport (details for horses, pigs, sheep and cattle), Report of the Scientific Committee on Animal Health and Animal Welfare, (2002) , pp. 130. Adopted on 11 March 2002 Accessed: 14th July 2017 https://ec.europa.eu/food/sites/food/files/safety/docs/sci-com_scah_out71_en.pdf.

[7] A.R. Elbers, et al., Tracing systems used during the epidemic of classical swine fever in the Netherlands, 1997-1998, Rev. Sci. Tech. 20 (2001) 614–629.

[8] H.C. de Carvalho Ferreira, E. Weesendorp, S. Quak, J.A. Stegeman, W.L. Loeffen, Quantification of airborne African swine fever virus after experimental infection, Vet. Microbiol. 165 (2013) 243–251.

[9] C. Alonso, et al., Evidence of infectivity of airborne porcine epidemic diarrhea virus and detection of airborne viral RNA at long distances from infected herds, Vet. Res. 45 (1) (2014) 5.

[10] J. Brackmann, Personal communication, Lower Saxony State Office for Consumer Protection and Food Safety, Germany, 2016.

[11] J. Gloster, L. Burgin, A. Jones, R. Sanson, Atmospheric dispersion models and their use in the assessment of disease transmission, Rev. Sci. Tech. 30 (2011) 457–465.

[12] G. Chen, et al., OpenFOAM for computational fluid dynamics, Not. Am. Math. Soc. 61 (4) (2014) 354–363.

[13] J. Seedorf, R.-G. Schmidt, Animal transport vehicles as potential bioaerosol emitters: A preliminary contribution to environmental hygiene by means of computational fluid dynamics (CFD) simulation, Berl. Münch. Tierärztl. Wochenschr. 130 (7/8) (2017) 285–292.

 http://dx.doi.org/10.1016/j.heliyon.2017.e00358

[14] C.A. Gilkeson, H.M. Thompson, M.C.T. Wilson, P.H. Gaskell, Quantifying passive ventilation within small livestock trailers using Computational Fluid Dynamics, Comput. Electron. Agri. 124 (2016) 84–99.

[15] I.E. Idelchik, Handbo ok of Hydraulic Resistance, Begell House, 1996.

[16] O.A. Mankowski, The wind tunnel simulation and effect of turbulent air flow on automotive aerodynamics, Durham theses, Durham University, 2013. Accessed: 19th May 2016 http://etheses.dur.ac.uk/10558/1/The_Wind_Tunnel_Simulation_and_Effect_of_Turbulent_Air_flow_on_Automotive_Aerodynamics_-_Oliver_Mankowski_2013.pdf.

[17] J. Tu, G.-H. Yeoh, C. Lin, Computational fluid dynamics: a practical approach, Elsevier, 2012.

[18] C.A. Gilkeson, H.M. Thompson, M.C.T. Wilson, P.H. Gaskell, R.H. Barnard, An experimental and computational study of the aerodynamic and passive ventilation characteristics of small livestock trailers, J. Wind Eng. Ind. Aerodyn. 97 (2009) 415–425.

[19] European Food Safety Authority, Standards for the microclimate inside animal road transport vehicles EFSA J. 122 (2004) 1–25.

[20] B. Predicala, A. Alvarado, S. Ekanayake, Field testing of an air filtration system for a pig transport trailer, Prairie Swine Centre Annual Research Report 2013-14, Canada, 2013, pp. 25–26. Accessed: 25th May 2015 http://www.prairieswine.com/wp-content/uploads/2014/12/Air-Filtration-Transport-Trailer.pdf.

[21] I.-H. Seo, et al., Aerosol emission from road by livestock transport vehicle movement, J. Korean Soc. Rural Plan. 19 (4) (2013) 137–147.

[22] W.-H. Hucho, Aerodynamics of road vehicles: From fluid mechanics to vehicle engineering, Society of Automotive Engineers, 1998.

[23] P.J. Kettlewell, et al., Design and operation of a prototype mechanical ventilation system for livestock transport vehicles, J. agric. Engng Res. 79 (2001) 429–439.

[24] P. Kettlewell, M. Mitchell, E. Harper, Guide to the ventilation of livestock during transport, (2017) . Accessed: 14th July 2017 http://www.jmrt.co.uk/pdf/Ventilation%20guide.pdf.

[25] C.R. Johnson, Visualization of Scalar and Vector Fields, (2012) . Accessed: 12th May 2017 http://www.sci.utah.edu/~chris/Johnson-Math-Encyclopedia/chapter.pdf.

 http://dx.doi.org/10.1016/j.heliyon.2017.e00358

[26] NASA, Uncertainty and error in CFD simulations, National Aeronautic and Space Administration, 2008. Accessed: 18th August 2016 https://www.grc.nasa.gov/WWW/wind/valid/tutorial/errors.html.

[27] J.P.G. Van Leuken, et al., Atmospheric dispersion modelling of bioaerosols that are pathogenic to humans and livestock −A review to inform risk assessment studies, Microb. Risk Anal. 1 (2016) 19–39.

[28] J. Schulz, et al., Longitudinal study of the contamination of air and of soil surfaces in the vicinity of pig barns by livestock-associated methicillin-resistant *Staphylococcus aureus*, Appl. Environ. Microbiol. 78 (2012) 5666–5671.

[29] D. Schley, L. Burgin, J. Gloster, Predicting infection risk of airborne foot-and-mouth disease, J. R. Soc. Interface 6 (2009) 455–462.

[30] J. Seedorf, J. Schulz, J. Hartung, Outdoor measurements of airborne emission of staphylococci from a broiler barn and its predictability by dispersion models, WIT Trans. Ecol. Envir. 85 (2005) 33–42.

[31] A. Ssematimba, T.J. Hagenaars, M.C.M. de Jong, Modelling the wind-borne spread of highly pathogenic avian influenza virus between farms, PLoS One 7 (2012) 9.

[32] L. Rong, P.V. Nielsen, B. Bjerg, G. Zhang, Summary of best guidelines and validation of CFD modeling in livestock buildings to ensure prediction quality, Comput. Electron. Agr. 121 (2016) 180–190.

[33] M. Shademan, R.M. Barron, R. Balachandar, Evaluation of OpenFOAM in academic research and industrial applications, 21st Conference of the CFD Society of Canada, At Sherbrooke, 6-9 May, Quebec, Canada, 2013, pp. 7. Accessed: 31th October 2015 http://www.researchgate.net/publication/261876529_Evaluation_of_OpenFOAM_in_Academic_Research_and_Industrial_Applications.

[34] E. Robertson, V. Choudhury, S. Bhushan, et al., Validation of OpenFOAM numerical methods and turbulence models for incompressible bluff body flows, Comput. Fluids 123 (2015) 122–145.

 http://dx.doi.org/10.1016/j.heliyon.2017.e00358